Highly Nitridated Graphene–Li_2S Cathodes with Stable Modulated Cycles

Yongcai Qiu, Genlan Rong, Jie Yang, Guizhu Li, Shuo Ma, Xinliang Wang, Zhenghui Pan, Yuan Hou, Meinan Liu, Fangmin Ye, Wanfei Li, Zhi Wei Seh, Xinyong Tao, Hongbin Yao, Nian Liu, Rufan Zhang, Guangmin Zhou, Jiaping Wang, Shoushan Fan, Yi Cui, and Yuegang Zhang**

The development of high-capacity cathode materials is critical for applications such as mobile devices and electric vehicles. Li/S batteries represent a promising system based on sulfur-conductive additive composite as the cathode.[1–5] However, various factors prevent the practical application of Li/S batteries,[5–12] including loss of the active sulfur material, volumetric change of the sulfur electrode, and shuttling effect between the negative and positive electrodes induced by the dissolution of intermediate polysulfides in the electrolyte. To address these key issues, much effort has been placed on encapsulating sulfur into conductive matrixes with porous structure and/or high surface to volume ratio, such as carbon nanotubes,[13,14] porous carbon,[15–17] graphene,[18–21] and carbon fibers.[22,23] For example, we previously found that cetyltrimethylammonium bromide (CTAB) modified graphene oxide (GO)–S nanocomposite cathode could significantly improve the cycle life of the Li/S cells to 1500 cycles.[24] Additionally, N-doped graphene (NG)–S composite cathode could reach the ultralong cycle life of the Li/S cells to 2000 cycles due to N functional groups of graphene which alleviate dissolution of polysulfides and help redisposition of polysulfides in the electrolyte.[25] It has also been reported recently that employing highly conductive metal oxides[26–28] or metal sulfides[29] are also an effective strategy for the redeposition of lithium polysulfides due to their affinities for these materials, which leads to significant improvement of corresponding Li/S cells.

Li_2S is a promising prelithiated cathode material with a high theoretical capacity of 1166 mA h g^{-1}. Unlike conventional sulfur cathode, Li_2S cathode shrinks as it delithiates initially, producing voids for subsequent lithiation/delithiation cycling, hence protecting the electrode structure from damage. More importantly, Li_2S can be matched with lithium metal-free anodes (such as silicon and tin), thus eliminating serious safety issues associated with the formation of "dendrites." Despite of these merits, the performance of Li_2S-based cathode significantly lags behind its sulfur counterpart.[9,10,30,31] A key issue for the Li_2S material seems to be in its inefficient activation and redeposition process.[32,33]

To understand the actual electrochemical activation processes, we first developed in situ scanning electron microscopy (SEM) and transmission electron microscopy (TEM) techniques to study the cathode material structural changes on delithiation. The newly developed in situ SEM set-up is shown in **Figure 1**a,b. A liquid cell contains one electrode with graphene and Li_2S particles on a 50 nm thick SiN_x window, and the other electrode with Li metal on Cu foil. The cell is filled by a liquid electrolyte (see the Experimental Section). When charged at 3.5 V, the conversion reaction from Li_2S to polysulfides occurs first at their surfaces (Figure 1c and Figure S1 and Movie 1, Supporting Information). We see that the Li_2S particles on graphene become smaller and smaller upon charging due to gradual dissolution of lithium polysulfides into the electrolyte. The phenomenon is also supported by in situ Raman spectroscopy (see Figure S2, Supporting Information). The observed phenomenon could be explained by that Li_2S was chemically converted to soluble lithium polysulfides upon charging. The process was further examined by in situ TEM study. A newly designed in situ TEM microchip (Figure 1d) was fabricated and schematically shown in Figure 1e. The main part is an Au wire, of which one end was connected to one electrode of the chip by silver paste, and the other end was glued with the graphene–Li_2S sample. The surface of the other electrode of the chip was deposited by Li metal. The graphene–Li_2S sample and Li metal were connected via an ionic liquid electrolyte. When charged at 3.5 V, Li_2S particles encapsulated in the graphene gradually disappeared (Figure 1f and Movie 2, Supporting Information). The processes could be explained by the dissolution of the generated lithium polysulfides in the ionic liquid electrolyte. The observed

Dr. Y. Qiu, G. Rong, J. Yang, G. Li, S. Ma, X. Wang, Z. Pan, Y. Hou, Dr. M. Liu, Dr. F. Ye, Dr. W. Li, Prof. Y. Zhang
i-Lab, Suzhou Institute of Nano-Tech and Nano-Bionics
Chinese Academy of Sciences
Suzhou, Jiangsu 215123, China
E-mail: ygzhang2012@sinano.ac.cn

Dr. Y. Qiu, Dr. Z. W. Seh, Prof. X. Tao, Dr. H. Yao, Dr. N. Liu, Dr. R. Zhang, Dr. G. Zhou, Prof. Y. Cui
Department of Materials Science and Engineering
Stanford University
Stanford, CA 94305, USA
E-mail: yicui@stanford.edu

Prof. J. Wang, Prof. S. Fan, Prof. Y. Zhang
Department of Physics
Tsinghua University
Beijing 100084, China

Prof. Y. Cui
Stanford Institute for Materials and Energy Sciences
SLAC National Accelerator Laboratory
2575 Sand Hill Road, Menlo Park, CA 94025, USA

DOI: 10.1002/aenm.201501369

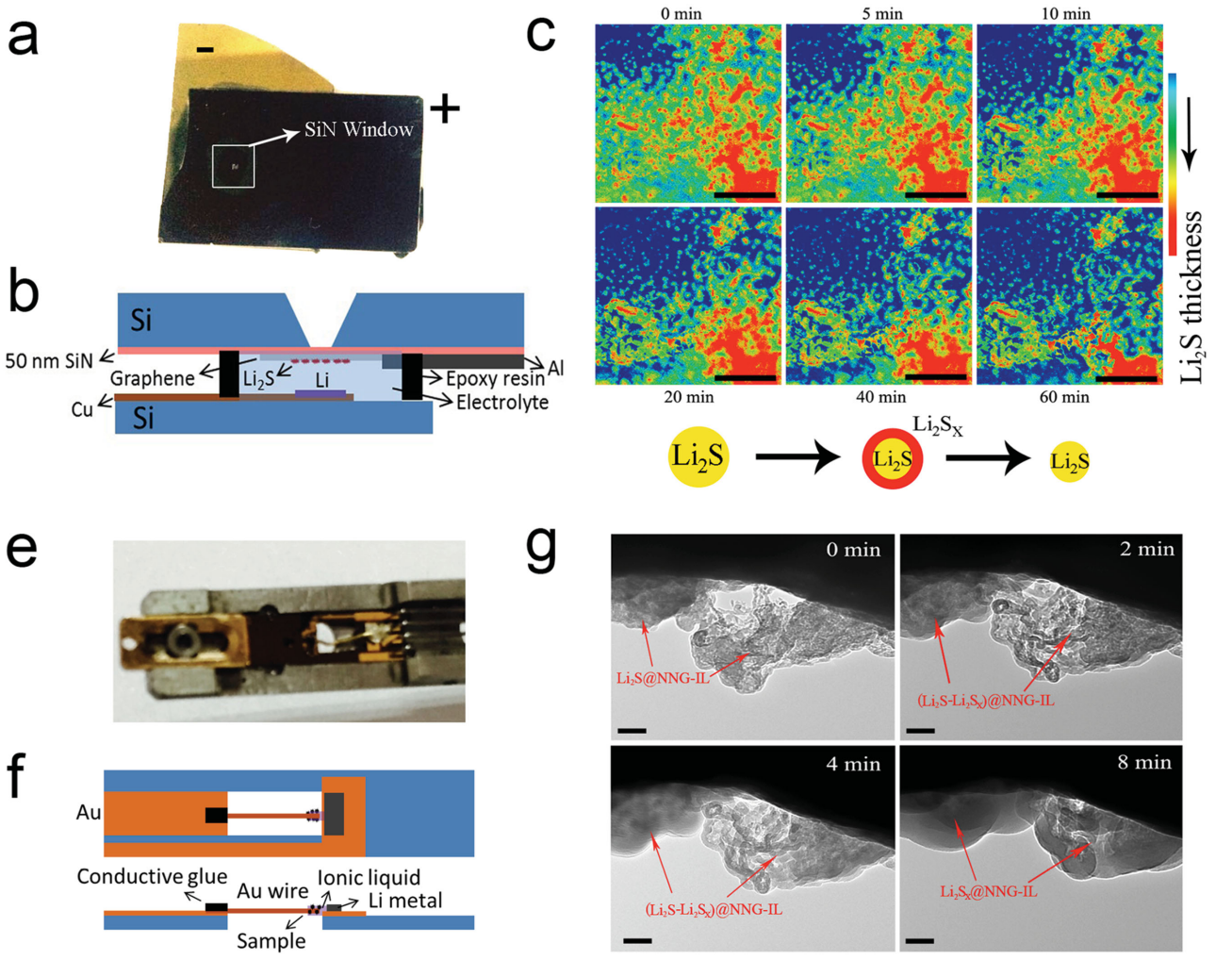

Figure 1. In situ electronic microscopy set-ups and the characterization results during delithiation of Li_2S. a,b) A newly developed electrochemical microcell for in situ SEM. c) Time-lapse SEM images of the activation process of Li_2S on a single-layered graphene electrode in a standard LiTFSI-DOL/DME electrolyte (also see Movie 1, Supporting Information). Red color shows a relatively thicker Li_2S layer on graphene. The Li_2S particles on graphene became smaller and smaller during the delithiation activation process, which was due to the continuous dissolution of the intermediate lithium polusulfides into the electrolyte (see schematic diagram below). Scale bar: 20 μm. d,e) An in situ TEM electrochemical characterization set-up. f) Time-lapse TEM images of the activation process of HNG–Li_2S in an ionic liquid based electrolyte (Movie 2, Supporting Information). Similarly, the generated intermediate lithium polysulfides during delithiation process gradually dissolved in the electrolyte, causing the aggregation of the HNG sheets and the remaining lithium sulfide or polysulfides. Scale bar: 50 nm.

slow aggregation of graphene sheets was due to the effect of the high-viscosity electrolyte. These results suggest that the activation of the Li_2S indeed involves dissolution processes. In other words, Li_2S in the Li_2S–C/Li cells will be redistributing upon charging/discharging. Therefore, to improve the performance of Li_2S cathode, creating a conductive matrix with functional groups that have strong affinity for redeposition of intermediate lithium polysulfides is the key.

Based on the above understanding, we explore the use of conductive and high-surface-area graphene to form a composite with Li_2S. Despite the previous research of using graphene and graphene oxides for S or Li_2S cathodes, we propose two novel approaches here to control the dissolution and redisposition processes of polysulfides in the electrolyte: (1) Significantly increasing the number of N functional sites in the NG-Li_2S composite, which would both increase the conductivity and provide more nucleation sites for intermediate polysulfides.[25] (2) Developing new charging procedures that would effectively redeposit the intermediate polysulfides.

A new-generation highly nitridated graphene (HNG) was synthesized with significantly enhanced amounts of N-functional groups. The HNG product was prepared by thermal nitridation of a graphene oxide/polyol mixture (see the Experimental Section and synthetic scheme in Figure S3, Supporting information). The HNG–Li_2S nanocomposite was experimentally realized following the steps as shown schematically in **Figure 2**a. First, the HNG structure presents more curvature and wrinkles as seen from TEM and SEM images (Figure S4, Supporting Information), which will bring out more cavities for locating Li_2S nanoparticles compared with the conventional NG sheets in previous reports.[25] The roles of nitrogen doping in improving electrochemical performance of electrodes have

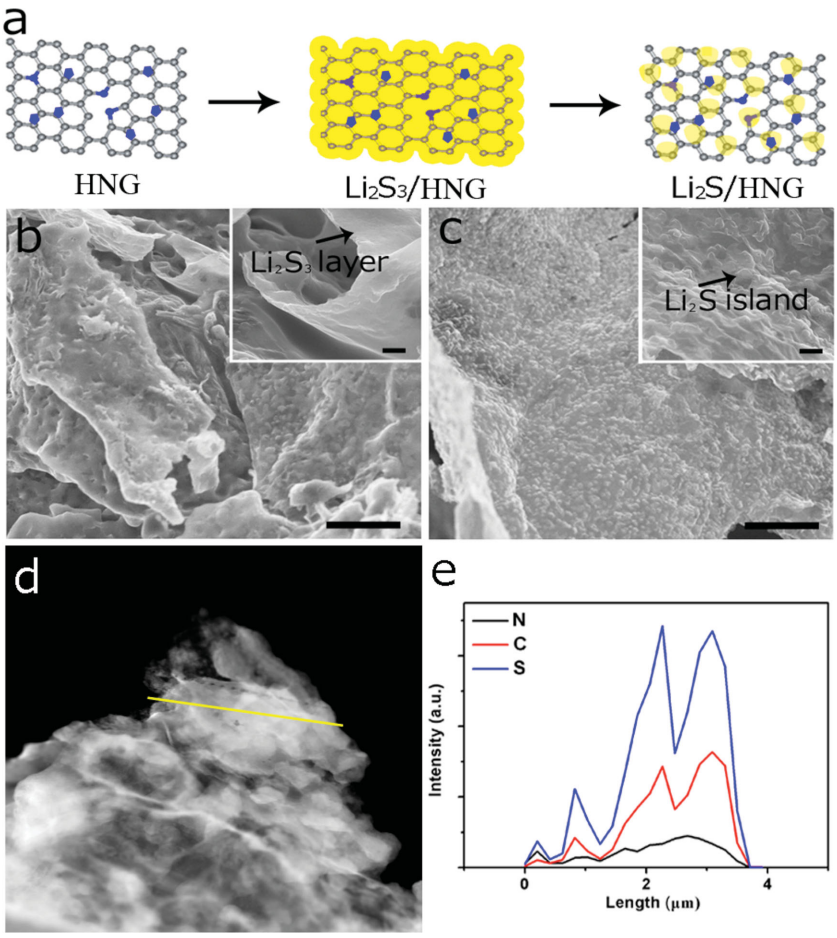

Figure 2. Synthesis and characterization of the HNG–Li_2S nanocomposite. a) Schematic illustration showing the preparation process of the HNG–Li_2S composite. b) Low- and high-magnification (the inset) SEM images of the HNG–Li_2S_3 composite, showing the layer-like Li_2S_3 coating on HNG. c) Low- and high-magnification (the inset) SEM images of the HNG–Li_2S composite, showing Li_2S islands distributed on HNG. The Li_2S islands were transformed from Li_2S_3 layers due to release of S during the heat treatment. d) Scanning TEM (STEM) image of the HNG–Li_2S composite and e) normalized EDX elemental profile along the line in (d). Scale bars in Figure 1b,c: 5 μm; others: 500 nm.

previously been demonstrated for supercapacitors and other energy storage devices.[34–38] In addition, the atomic nitrogen to carbon ratio (N/C) in the HNG sheets is estimated to be ≈12.2% from the X-ray photoelectron spectroscopic (XPS) peak areas of C 1s and N 1s (**Figure 3**a), which is more than three times higher than that in the previous report.[25] Second, amorphous Li_2S_3 can be coated on both sides of HNG to form sandwich structures by solvent evaporation, as validated by XRD patterns (Figure 3b) and SEM characterization (Figure 2b). Finally, Li_2S_3 can be transformed into cubic Li_2S by heat treatment at 300 °C for 1 h, as validated by XRD patterns in Figure 3b. The sharp diffraction peaks and absence of impurity peaks indicate the high crystallinity and high purity of the Li_2S product. Raman spectrum of the HNG–Li_2S product also indicates the existence of Li_2S phase (Figure S5, Supporting Information).[11] Interestingly, during the phase transition, the layer-like morphology of Li_2S_3 changes into Li_2S islands which have an average grain size of 500 nm and are well dispersed on HNG sheets (Figure 2c,d).

Shown in Figure 2e is a line scan of normalized energy dispersive X-ray (EDX) spectral peak intensities taken from Figure 2d, indicating that carbon, nitrogen, and sulfur are uniformly dispersed in the composite material, which are further supported by the SEM EDX elemental mapping (Figure S6, Supporting Information). Thermogravimetric analysis (TGA) indicates the nanocomposite contains ≈66.3 wt% of Li_2S (Figure S7, Supporting Information). To make a slurry for electrodes, the HNG–Li_2S nanocomposite was directly mixed with 5 wt% polyvinylpyrrolidone (PVP) binder without adding any extra carbon black. The slurry was then spread evenly on superaligned carbon nanotube array (SCNTA, see Figure S8, Supporting Information) current collectors with an average Li_2S loading of ≈1.2 mg cm^{-2} (≈60% Li_2S in the entire electrode), which were heated at 100 °C for 10 h under vacuum before using as electrodes for coin cell assembly.

Cyclic voltammetry (CV) of HNG–Li_2S cathode was performed with an initial charge to 3.8 V versus Li/Li^+ to activate Li_2S, followed by cycling in a potential range from 1.5 to 2.8 V at a scan rate of 0.1 mV s^{-1} (Figure S9, Supporting Information).[39] The first anodic scan shows two broad oxidation peaks centered at 2.69 and 3.54 V, respectively, corresponding to electrochemical conversion of Li_2S to S or polysulfides, which is similar to our previous reports and other references based on Li_2S–C cathodes.[3] The subsequent cathodic scan shows two broad reduction peaks centered at 2.23 and 1.99 V, respectively, corresponding to transformation of polysulfides or S into Li_2S. The reversible processes are found in the following cycles. It is worth noting that the two reduction peaks in the subsequent cycles shift to higher potentials at 2.24 and 2.03 V, respectively, and one oxidation peak shifts back to 2.41 V, indicating a reduced polarization after the first delithiated cycle. The rate performance of the HNG–Li_2S/Li cells was investigated by galvanostatic discharge/charge (Figure S9, Supporting Information). The 1 C-rate is defined as the current density of 1166 mA g^{-1} (by Li_2S weight). After the first charge with a specific capacity of ≈1074 mA h g^{-1} (by Li_2S weight, equivalent to 1545 mAh g^{-1} of S) at a rate of 0.05 C, the cell can deliver a specific discharge capacity of ≈1067 mA h g^{-1}, nearly 91.5% of the theoretical capacity of Li_2S (see the first charge/discharge curves in Figure S10a (Supporting Information). When the rate is changed to 0.1 C, a specific capacity of ≈926 mAh g^{-1} of Li_2S is retained. Upon increasing the rate, the capacities exhibited were ≈817 mA h g^{-1} at 0.2 C, ≈716 mA h g^{-1} at 0.5 C, ≈629 mA h g^{-1} at 1 C, ≈533 mA h g^{-1} at 2 C, ≈361 mA h g^{-1} at 5 C, ≈233 mA h g^{-1} at 10 C, and finally recovered to ≈795 mA h g^{-1} at a rate of 0.2 C. Interestingly, as

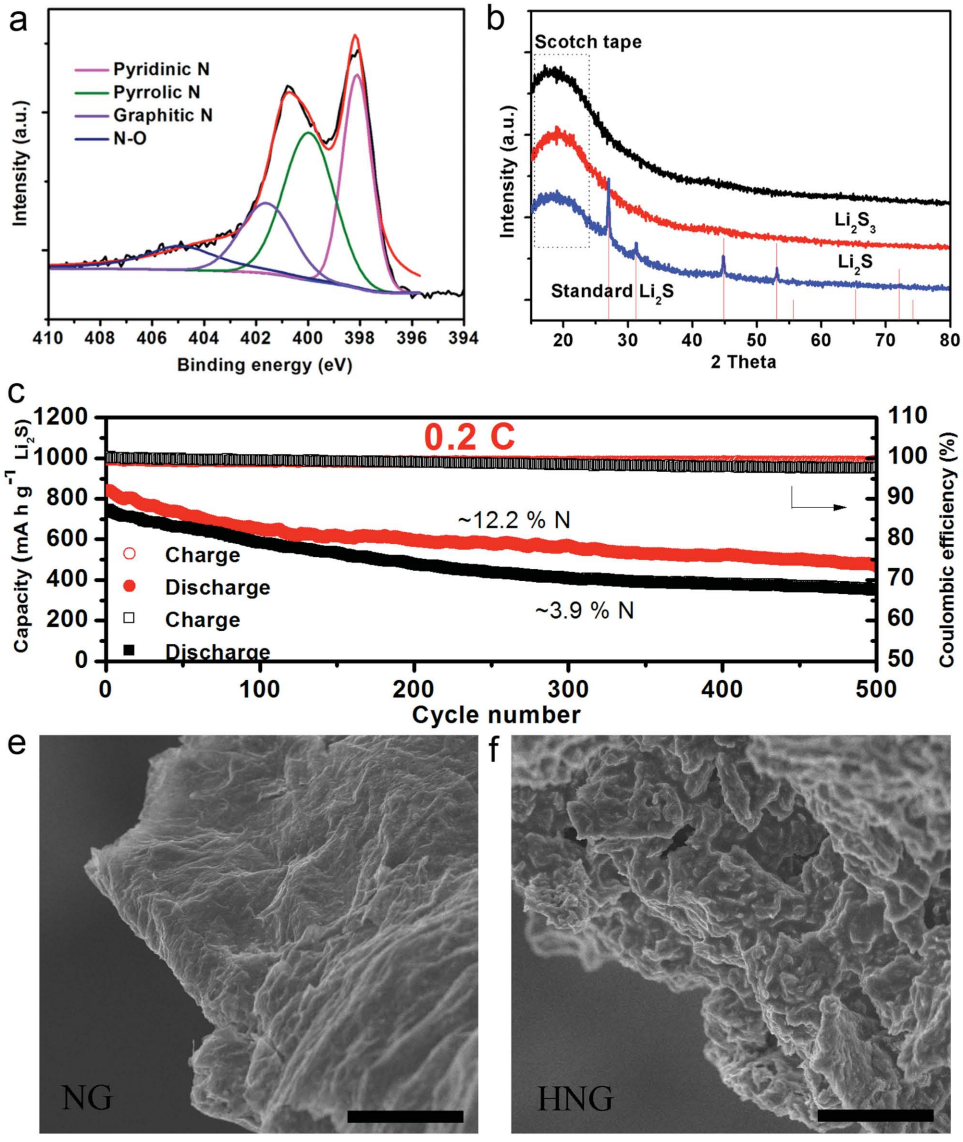

Figure 3. Characterization and electrochemical measurements of the HNG–Li_2S/Li cells. a) High-resolution XPS spectrum of the HNG powder. The evaluated N content is ≈12.2 wt% in HNG. The pyridinic N and pyrrolic N are dominant, which is helpful for preventing polysulfides from shuttling. b) XRD patterns of the as-obtained HNG–Li_2S_3 and HNG–Li_2S powder. After thermal treatment, amorphous Li_2S_3 can be transformed into cubic Li_2S. d,e) Li_2S particles formed on the NG and HNG electrode surface at fully discharge state (1.7 V). As seen, more Li_2S particles were readily formed on the HNG electrode surface, suggesting that the N functional groups are effective in reusing lithium polysulfide dissolve in electrolyte. Scale bars in (d) and (e): 5 μm.

seen in Figure S10b (Supporting Information), the main discharge voltage plateau stays above 2.0 V even at 2 C, indicative of a good conductive network for electrochemical reactions, which is likely due to the synergic effect of SCNTA and HNG.

We have demonstrated that the N functional groups are effective in preventing lithium polysulfide shuttling for the cells (Figure 3c). As seen, the NG–Li_2S/Li cell delivers an initial discharge capacity of ≈730 mA h g^{-1} of Li_2S and a capacity of about 356 mA h g^{-1} of Li_2S after 500 cycles, and a capacity decay of 0.16% per cycle. The Coulombic efficiency is as low as 97% after 500 cycles, and that the trend is more and more serious. The performance is much lower than the HNG–Li_2S/Li cell (remaining 480 mA h g^{-1} of Li_2S after 500 cycles), further indicating that N functional groups are effective in reusing lithium polysulfide dissoluble in electrolyte. This is also demonstrated by examining Li_2S deposition on HNG and NG electrodes (cells were charged to 3.8 V and then discharged to 1.7 V). As seen in Figure 3d,e, in contrast to the NG electrode at the fully discharged state, more Li_2S particles were readily formed on the HNG electrode surface. These results further suggested that the new-generation HNG sheets could play an important role similar to a "self-healing" agent for the electrode, which makes it a promising matrix material for fabricating high performance Li_2S cathode. However, even with these improvements, the demonstrated cycling stability is still not good enough for practical applications. Therefore, we used

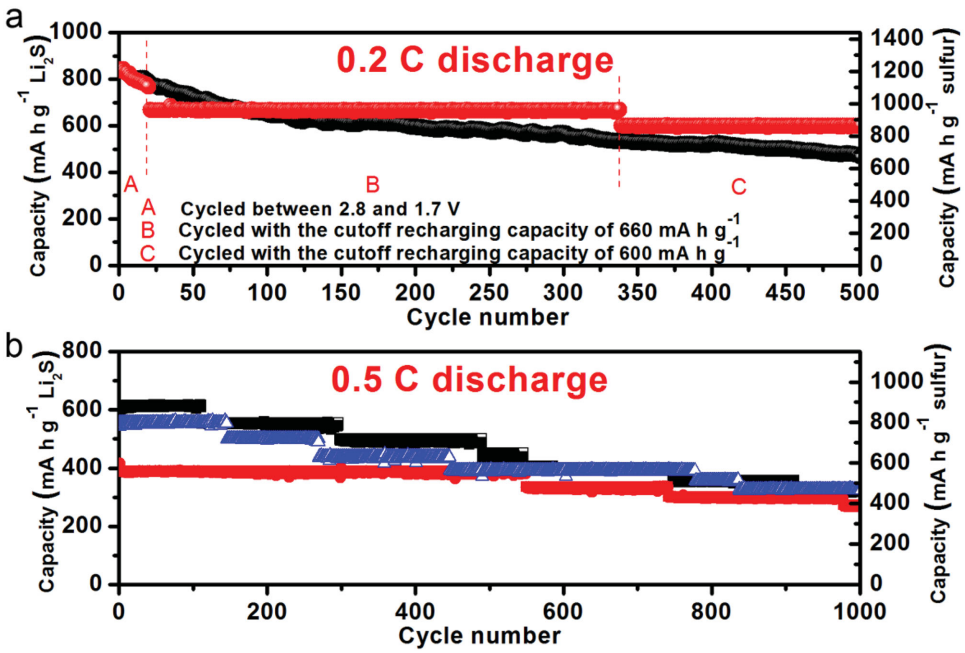

Figure 4. Cycling performance of the HNG–Li_2S/Li cells. a) Performance comparison between a cell with the conventional charge procedure (black, initially charged to 3.8 V and then cycled between 1.7 to 2.8 V at 0.2 C) and another cell with the modified charge procedure (red, limiting recharge capacity to the specified values with a cutoff voltage of 2.4 V; the detailed protocol is described in the main text). An improved cycling performance is demonstrated for the cell with the specific recharge control. b) Performance comparison between the cells using the modified charge procedures with different initial cutoff recharge capacities (the detail protocols are described in the main text). The best overall capacity retention was achieved with the cell using the highest initial cutoff capacity setting.

a more sophisticated recharge modulation protocol to further improve the performance of the HNG–Li_2S/Li cells.

The modulation of charge capacity or voltage window is an effective strategy for stabilizing the cathode reactions, which has been widely utilized in lithium-ion batteries. Although there are a few reports on restricting the charge capacity in Li/S batteries,[36] there is not yet a successful case for a Li_2S based cell to achieve the high capacity and long cycle-life using a recharge modulation protocol until now. In general, restricting the voltage window can avoid some side reactions in a battery system. For the Li/S battery system, limiting the charge capacity and its voltage window can alleviate dissolution of polysulfides. The Li/S cells are typically operated between 2.8 and 1.7 V. The formation of polysulfides (Li_2S_8, Li_2S_6 and Li_2S_4) usually occurs in the voltage range between 2.8 and ≈2.2 V (≈25% of the total capacity). The long-chain lithium polysulfides such as Li_2S_8 and Li_2S_6 are highly dissoluble in ether-based electrolytes, which can cause rapid capacity fading during cell cycling. The conversion from Li_2S_4 to Li_2S and/or the redeposition of Li_2S from polysulfides in the electrolyte takes place in the voltage range between ≈2.2 and 1.7 V.[39–48] The capacity at this stage (≈75% of the total capacity) is relatively stable as the short-chain lithium polysulfides have low solubility in the electrolyte. Therefore, we take two approaches to achieve long cycle-life Li/S cells: one is increasing the number of active sites for redepositing Li_2S from polysulfides in the electrolyte (see Figure 3d), the other is limiting the charge voltage range for inhibiting the dissolution of long-chain lithium polysulfides in the electrolyte.

Figure 4a shows the performance comparison between a cell using the standard recharge procedure (cycled between 2.8 and 1.7 V after the first charge to 3.8 V at 0.05 C) and another cell using the modified recharge procedure with a protocol to limit is charge capacity and voltage (cycled between 2.8 and 1.7 V over 20 cycles at 0.2 C after the first charge to 3.8 V at 0.05 C; set a cutoff recharge capacity of 660 mA h g^{-1} of Li_2S and continued to cycle until the charge potential increased to ≈2.4 V; reset the cutoff recharge capacity to 600 mA h g^{-1} of Li_2S and continued to cycle). Reducing recharge capacity leads to a lower charge voltage plateau (see Figure S11, Supporting Information). In this way, a certain amount of unreacted Li_2S might be retained and play a crucial role as nucleation seeding sites to facilitate the precipitation of Li_2S and the adsorption of soluble lithium polysulfides. As seen in Figure 4a, the trend of capacity decay for the two cells is almost identical before 20 cycles. The cell using the standard recharge procedure can deliver a specific capacity of ≈534 mA h g^{-1} after 500 cycles, corresponding to a capacity decay of 0.13% per cycle. As for 500 cycles, the total charge capacities and total discharge capacities are 297 920 and 294 336 mA h g^{-1}, respectively, corresponding to an average Coulombic efficiency of 98.8% (see Figure S12a, Supporting Information). By contrast, the cell using the modified recharge procedure can deliver a specific capacity of ≈596 mA h g^{-1} (≈857 mAh g^{-1} of S) after 500 cycles, corresponding to a capacity loss of 0.089% per cycle. The total charge capacities and total discharge capacities in 500 cycles are 326 820 and 324 196 mAh g^{-1}, respectively, corresponding to an average Coulombic efficiency of 99.2% (see Figure S12a, Supporting Information). The

results thus indicate the control of the cutoff recharge capacity and voltage can significantly enhance the capacity and cycling stability of the HNG–Li_2S/Li cells.

Figure 4b shows the long-term cycling performance comparison of the HNG–Li_2S/Li cells using the modified recharge procedures with different initial cutoff recharge capacities (610, 555, and 389 mA h g^{-1}, respectively, and all discharged at a rate of 0.5 C). As seen, the cell with the lower initial cutoff recharge capacity exhibits longer cycling stability at the first capacity-controlled stage. With limiting charge voltage to 2.4 V, the cell can sustain 112 cycles with the cutoff recharge capacity of 610 mA h g^{-1} (≈878 mA h g^{-1} of S), 148 cycles with the cutoff recharge capacity of 555 mA h g^{-1} (≈798 mAh g^{-1} of S), and 545 cycles with the cutoff recharge capacity of 389 mA h g^{-1} (≈560 mAh g^{-1} of S). Subsequently, these cells were switched to a procedure in which the cutoff recharge capacity of each following stage resets to 90% of the current cutoff capacity whenever the charge voltage reached to 2.4 V, but under otherwise identical conditions. In this way, they can continue to output highly stable capacity for several hundreds of cycles. As a final comparison result, the cell with a higher initial cutoff recharge capacity can deliver higher overall stable capacity. More impressively, the cells with different recharge capacities all exhibit high average Coulombic efficiencies of more than 97% over 1000 cycles (see Figure S12b, Supporting Information).

Furthermore, high-rate and ultralong cycle-life HNG–Li_2S/Li cells can be achieved with the specific recharge procedure, as shown in (see Figure S12c,d, Supporting Information). When discharged at 1 C, the cell can still deliver a specific capacity of ≈318 mA h g^{-1} (≈457 mAh g^{-1} of S) after 2000 cycles, which is much higher than that using the traditional recharge procedure (≈115 mA h g^{-1} evaluated from the decay slope before 230 cycles). More impressively, when discharged at 2 C, the cell could deliver a specific capacity of ≈256 mA h g^{-1} (≈368 mAh g^{-1} of S) after 3000 cycles. This value is higher than that of the most state-of-the-art Li-ion cells. The average Coulombic efficiency of the cells is 97.8% over 2000 cycles at 1 C, and 98.3% over 3000 cycles at 2 C (see Figure S12, Supporting Information), suggesting that the polysulfide shuttling effect could be more effectively restrained at a higher current rate because of the faster discharge/charge process. The good cycling results could be explained by the factor that the capacity and voltage modulation prevents the formation of highly soluble long-chain polysulfides, and always keeps a certain amount of insoluble Li_2S located on HNG, which is useful for redeposition of Li_2S and the adsorption of soluble intermediate polysulfides and thereby achieving highly stable capacity retention for hundreds or even thousands of cycles.

In conclusion, utilizing a new-generation highly nitridated graphene as conductive matrix for Li_2S and a capacity-modulation and voltage-modulation recharge procedure, we achieved highly stable HNG–Li_2S/Li cells for hundreds of, even thousands of cycles. By optimizing Li_2S redeposition sites and preventing the dissolution of long-chain polysulfides, a stable specific capacity of ≈318 mA h g^{-1} (≈457 mAh g^{-1} of S) at 1 C still remains after 2000 cycles, even a stable specific capacity of ≈256 mA h g^{-1} (≈368 mAh g^{-1} of S) retains at 2 C after 3000 cycles, which is perhaps the longest cycle life demonstrated so far (see Table S1, Supporting Information). These results were achieved based on our understanding of the Li_2S dissolution-redeposition mechanism revealed by our in situ SEM and TEM observations. We also found that the insoluble Li_2S residual during our modulated charge process could have two-side effects: the positive side is that it can be used as seeds for redeposition of Li_2S and adsorption of soluble intermediate polysulfides; the negative side is that extra inactive Li_2S could build up and cause capacity loss, which could only be resolved by an additional reactivation procedure (see Figure S13, Supporting Information). The new electrode material design and the new recharge protocol could open a promising avenue for the practical implementation of high-energy density Li_2S–C/Li cells.

Experimental Section

Synthesis of the New-Generation Highly Nitridated Graphene (HNG): GO was synthesized according to the literature reported by Xu et al. Briefly, natural graphite powder (20 g) was put into an 80 °C solution of concentrated H_2SO_4 (30 mL), $K_2S_2O_8$ (10 g), and P_2O_5 (10 g), and then kept for 6 h to preoxidize the graphite powder. After cooling to room temperature, 3.5 L deionized (DI) water was added into the mixture, which was then filtrated, washed, and vacuum dried before storage. Subsequently, the dried preoxidized graphite was oxidized using a modified Hummers' method: First, the preoxided graphite powder (0.5 g) was put into concentrated H_2SO_4 (12 mL, 0 °C), followed by gradually adding $KMnO_4$ (1.5 g) under vigorous stirring. Second, the mixture was stirred at 35 °C for 2 h, and then diluted with DI water (24 mL). Successively, the resultant mixture was stirred at an elevated temperature of 80 °C for 0.5 h. After cooling to room temperature, an additional 70 mL DI water was added, and shortly, 1.25 mL 30% H_2O_2 was added. Finally, the mixture was washed with 5 wt% HCl aqueous solution (125 mL) to remove metal ions, followed by washing with DI water three times and centrifugation. Dialysis was carried out to further remove the remaining metal species.

For polyol modification, the as-obtained GO were first coated with glucose molecules. Briefly, 1 g glucose was added into 1000 mL of GO suspension (0.2 mg mL^{-1}), followed by stirring for 30 min. Then, 1.5 mL of ammonia solution (25%–28%) was added into the resulting dispersion. The mixture was stirred for 2 h at 95 °C. To precipitate the GO/glucose solution, 20 mg of cetyltrimethylammonium bromide (CTAB) was added and continued to stir. The precipitated sample was filtered and rinsed several times by distilled water to remove excess glucose and CTAB. The black GO/glucose powder was dried overnight in a vacuum oven at 60 °C.

The HNG powder was obtained by nitridation treatment of the dried GO/polyol product. Briefly, the freeze dried GO/polyol powder was loaded into a silica tube reactor placed in a horizontal tube furnace and connected to a gas feed system. Initially, a flow of Ar gas (99.99%) was maintained over the bed to get rid of air and H_2O. Then the flowing gas was switched to NH_3 with a flow rate of 30 cm^3 min^{-1}. The furnace was heated from room temperature to 750 °C at a rate of 30 °C min^{-1}, held at this temperature for 30 min. Finally, the furnace was allowed to cool down under a flowing Ar gas. The synthesis of NG powder can be found in our previous report.[25]

Synthesis of HNG–Li_2S and NG–Li_2S Nanocomposites: An absolute ethanol solution of Li_2S_3 was first prepared by the mixture of Li_2S and S in a molar ratio of 1:2. Then, the dried HNG powder was added into the above clear yellow Li_2S_3 solution and was stirred for 30 min. Afterward, the dried HNG–Li_2S_3 powder was obtained by evaporation of ethanol at 80 °C. Finally, the HNG–Li_2S composite was obtained by thermal decomposition of HNG–Li_2S_3 powder at 300 °C for 1 h. For preparation of NG–Li_2S nanocomposite, the same procedure was used except that

HNG powder was replaced with NG powder. Due to the sensitivity of Li_2S to moisture, all the electrode preparation procedures were carried out in an argon-filled glove box with moisture of <1 ppm.

Electrochemical Measurements: To prepare the cathodes, the HNG–Li_2S composite materials were first mixed with PVP binder (95:5 by weight) in 1-Methyl-2-pyrrolidone (NMP) solution under vigorous stirring overnight. The mixture was then spread evenly on the superaligned carbon nanotube arrays and roll-pressed to produce electrode films with an average Li_2S loading of 1.2 mg cm^{-2}, which were heated at 100 °C for 10 h under vacuum before using to fabricate the coin cells. To test the electrochemical performance, the HNG–Li_2S–SCNTA electrode was assembled into CR2025 coin-type cells with Li electrode and electrolyte (LiTFSI (1 M), $LiNO_3$ (1 wt%) and 0.025 M Li_2S_8 in 1,3-dioxolane (DOL)/1,2-dimethoxyethane (DME) solvent) in an Ar-filled glove box. $LiNO_3$ additive added to the electrolyte is to passivate the lithium anode surface and thus reduce the shuttle effect. A certain amount of Li_2S_8 additive was added to the electrolyte as it has a positive effect on improvement of cycling stability. The total amount of sulfur in the polysulfide additive is about 9.2 wt% of that in the entire cell. Specific capacity values are calculated based on the total S weight included both in the HNG–Li_2S and in Li_2S_8 additive. The electrolyte solution was prepared by dissolving stoichiometric amount of Li_2S and sulfur (nominal Li_2S_8, [S] = 0.2 M) in commercial LiTFSI (1 M in DOL/DME) and $LiNO_3$ (1 wt%). 20 µL of the electrolyte (≈0.188 mg Li_2S) was added to assemble each cell.

In Situ *SEM and TEM*: The in situ SEM cell set-up was shown in Figure 1a and schematically shown in Figure 1b. The all chips used in this work were fabricated in a cleanroom. A 50 nm Si-rich layer of SiN_x was grown on a thick silicon wafer by low-pressure chemical vapor deposition. Windows were created using photolithography and reactive ion etching to open the SiN_x on reverse side of the wafer and removing the silicon between the reverse side and the front side by anisotropic KOH etch. Graphene electrode was transferred onto the SiN_x window and then deposited Al metal with a shadow mask to leave the transparent SiN_x/graphene window. One drop of Li_2S dissolved in absolute ethanol was added on the chip with the SiN_x/graphene layer, which was then heated at 80 °C for 30 min. The other side of the chips was directly deposited Cu metal by evaporation. The middle of the chip was bound by Li metal. A sandwich structure was assembled using the two different chips in an argon-filled glove box with the middle filled with electrolyte (LiTFSI (1 M) in DOL/DME solvent).

The in situ TEM cell set-up was shown in Figure 1d and schematically shown in Figure 1e. The chips with two separated electrode patterns were designed and used in a specialized electrical biasing holder (DENSsolutions). The main part is an Au wire. One terminal was connected to one electrode of the chip by silver paste, and the other end was glued with HNG–Li_2S sample. The surface of another electrode of the chip was deposited by Li metal. The sample and Li metal was connected via ionic liquid electrolyte. An ionic liquid electrolyte (1 M) containing lithium bis(trifluoromethane sulfonyl)imide (LiTFSI) in a solvent of 1-butyl-1-methylpyrrolidinium bis(trifluoromethane sulfonyl) imide (Py_{14}TFSI) was used. By biasing the working electrode between 3.5 V versus the counter electrode, Li ions extract from Li_2S and flow toward Li metal electrode.

Material Characterization: SEM was measured on a Quanta 400 FEG field-emission scanning electron microscope and a Quanta 250 environmental scanning electron microscope. XRD was collected with a Bruker D8 diffractometer. TEM was measured on a Tecnai G2 F20 S-Twin field-emission transmission electron microscope. TG measurement was performed using a TG/DTA 6200. Electrochemical measurements were carried out using a Land CT2001 automatic battery tester.

Supporting Information

Supporting Information is available from the Wiley Online Library or from the author.

Acknowledgements

This work was supported by the National Natural Science Foundation of China (21433013 and 21403287), the National Science Foundation for Post-doctoral Scientists of China (014M550314), the Natural Science Foundation of Jiangsu Province, China (BK20140383), and the Science and technology development program in Suzhou (SYG201532).

Received: July 8, 2015
Revised: August 13, 2015
Published online: September 21, 2015

[1] A. Manthiram, Y. Fu, S. H. Chung, C. Zu, Y. S. Su, *Chem. Rev.* **2014**, *114*, 11751.
[2] Y. Yang, G. Zheng, Y. Cui, *Chem. Soc. Rev.* **2013**, *42*, 3018.
[3] K. Cai, M.-K. Song, E. J. Cairns, Y. Zhang, *Nano Lett.* **2012**, *12*, 6474.
[4] C. Wang, X. Wang, Y. Yang, A. Kushima, J. Chen, Y. Huang, J. Li, *Nano Lett.* **2015**, *15*, 1796.
[5] M. K. Song, E. J. Cairns, Y. Zhang, *Nanoscale* **2013**, *5*, 2186.
[6] M. Nagao, A. Hayashi, M. Tatsumisago, *J. Mater. Chem.* **2012**, *22*, 10015.
[7] J. Hassoun, B. Scrosati, *Angew. Chem. Int. Ed.* **2010**, *49*, 2371.
[8] Z. Lin, Z. Liu, N. J. Dudney, C. Liang, *ACS Nano* **2013**, *7*, 2829.
[9] Y. Fu, Y.-S. Su, A. Manthiram, *Adv. Energy Mater.* **2014**, *4*, 1300655.
[10] Z. W. Seh, H. Wang, P. Hsu, Q. Zhang, W. Li, G. Zheng, H. Yao, Y. Cui, *Energy Environ. Sci.* **2014**, *7*, 672.
[11] Z. W. Seh, H. Wang, N. Liu, G. Zheng, W. Li, H. Yao, Y. Cui, *Chem. Sci.* **2014**, *5*, 1396.
[12] Y. C. Qiu, W. Li, G. Li, Y. Hou, L. Zhou, H. Li, M. Liu, F. Ye, X. Yang, Y. Zhang, *Nano Res.* **2014**, *7*, 1355.
[13] Y. S. Su, Y. Fu, A. Manthiram, *Phys. Chem. Chem. Phys.* **2012**, *14*, 14495.
[14] J. Guo, Y. Xu, C. Wang, *Nano Lett.* **2011**, *11*, 4288.
[15] X. Ji, K. T. Lee, L. F. Nazar, *Nat. Mater.* **2009**, *8*, 500.
[16] D. S. Jung, T. H. Hwang, J. H. Lee, H. Y. Koo, R. A. Shakoor, R. Kahraman, Y. N. Jo, M.-S. Park, J. W. Choi, *Nano Lett.* **2014**, *14*, 4418.
[17] N. Jayaprakash, J. Shen, S. S. Moganty, A. Corona, L. A. Archer, *Angew. Chem. Int. Ed.* **2011**, *50*, 5904.
[18] L. Ji, M. Rao, H. Zheng, L. Zhang, Y. Li, W. Duan, J. Guo, E. J. Cairns, Y. Zhang, *J. Am. Chem. Soc.* **2011**, *133*, 18522.
[19] H. Chen, C. Wang, W. Dong, W. Lu, Z. Du, L. Chen, *Nano Lett.* **2015**, *15*, 798.
[20] G. Zhou, L.-C. Yin, D.-W. Wang, L. Li, S. Pei, I. R. Gentle, F. Li, H.-M. Cheng, *ACS Nano* **2013**, *7*, 5367.
[21] H. Li, X. Yang, X. Wang, M. Liu, F. Ye, J. Wang, Y. Qiu, W. Li, Y. Zhang, *Nano Energy* **2015**, *12*, 468.
[22] L. Ji, M. Rao, S. Aloni, L. Wang, E. J. Cairns, Y. Zhang, *Energy Environ. Sci.* **2011**, *4*, 5053.
[23] G. Zheng, Q. Zhang, J. J. Cha, Y. Yang, W. Li, Z. W. Seh, Y. Cui, *Nano Lett.* **2013**, *13*, 1265.
[24] M. K. Song, Y. Zhang, E. J. Cairns, *Nano Lett.* **2013**, *13*, 5891.
[25] Y. Qiu, W. Li, W. Zhao, G. Li, Y. Hou, M. Liu, L. Zhou, F. Ye, H. Li, Z. Wei, S. Yang, W. Duan, Y. Ye, J. Guo, Y. Zhang, *Nano Lett.* **2014**, *14*, 4821.
[26] Z. W. She, W. Li, J. J. Cha, G. Zheng, Y. Yang, M. T. McDowell, P.-C. Hsu, Y. Cui, *Nat. Commun.* **2013**, *4*, 1331.
[27] Z. Liang, G. Zheng, W. Li, Z. W. Seh, H. Yao, K. Yan, D. Kong, Y. Cui, *ACS Nano* **2014**, *8*, 5249.
[28] H. Yao, G. Zheng, P.-C. Hsu, D. Kong, J. J. Cha, W. Li, Z. W. She, M. T. McDowell, K. Yan, Z. Liang, V. Narasimhan, Y. Cui, *Nat. Commun.* **2014**, *5*, 3943.

[29] Z. W. Seh, J. H. Yu, W. Li, P.-C. Hsu, H. Wang, Y. Sun, H. Yao, Q. Zhang, Y. Cui, *Nat. Commun.* **2014**, *5*, 5017.
[30] L. Chen, Y. Liu, M. Ashuri, C. Liu, L. L. Shaw, *J. Mater. Chem. A* **2014**, *2*, 18026.
[31] X. Meng, D. J. Comstock, T. T. Fister, J. W. Elam, *ACS Nano* **2014**, *8*, 10963.
[32] Y. Yang, G. Zheng, S. Misra, J. Nelson, M. F. Toney, Y. Cui, *J. Am. Chem. Soc.* **2012**, *134*, 15387.
[33] Y. Yang, M. T. McDowell, A. Jackson, J. J. Cha, S. S. Hong, Y. Cui, *Nano Lett.* **2010**, *10*, 1486.
[34] Y. Qiu, X. Zhang, S. Yang, *Phys. Chem. Chem. Phys.* **2011**, *13*, 12554.
[35] H. Jeong, J. Lee, We. Shin, Y. Choi, H. Shin, J. Kang, J. Choi, *Nano Lett.* **2011**, *11*, 2472.
[36] S. Wu, R. Xu, M. Lu, R. Ge, J. Iocozzia, C. Han, B. Jiang, Z. Lin, *Adv. Energy Mater.* **2015**, *5*, 1500400.
[37] X. Zhou, J. Qiao, L. Yang, J. Zhang, *Adv. Energy Mater.* **2014**, *4*, 1301523.
[38] J. Yan, Q. Wang, T. Wei, Z. Fan, *Adv. Energy Mater.* **2013**, *3*, 1300816.
[39] C.-N. Lin, W.-C. Chen, Y.-F. Song, C.-C. Wang, L.-D. Tsai, N.-L. Wu, *J. Power Sources* **2014**, *263*, 98.
[40] Y. Diao, K. Xie, X. Hong, S. Xiong, *Acta Chim. Sinica* **2013**, *71*, 508.
[41] Y. S. Su, Y. Fu, T. Cochell, A. Manthiram, *Nat. Commun.* **2013**, *4*, 2985.
[42] W. Li, G. Zheng, Y. Yang, Z. W. Seh, N. Liu, Y. Cui, *Proc. Natl. Acad. Sci. USA* **2013**, *110*, 7148.
[43] S. Lu, Y. Cheng, X. Wu, J. Liu, *Nano Lett.* **2013**, *12*, 2485.
[44] Q. Zhao, X. Hu, K. Zhang, N. Zhang, Y. Hu, J. Chen, *Nano Lett.* **2015**, *15*, 721.
[45] J. Xu, J. Shui, J. Wang, M. Wang, H. Liu, S. X. Dou, I.-Y. Jeon, J.-M. Seo, J.-B. Baek, L. Dai, *ACS Nano* **2014**, *8*, 10920.
[46] R. Xu, J. Lu, K. Amine, *Adv. Energy Mater.* **2015**, *5*, 1500408.
[47] G. Zhou, Y. Zhao, A. Manthiram, *Adv. Energy Mater.* **2015**, *5*, 1402263.
[48] S. Chen, X. Huang, H. Liu, B. Sun, W. Yeoh, K. Li, J. Zhang, G. Wang, *Adv. Energy Mater.* **2014**, *4*, 1301761.